

# Boosting indirect detection of secluded dark matter sector

Jinmian Li,<sup>1,\*</sup> Takaaki Nomura,<sup>1,†</sup> Junle Pei,<sup>2,3,‡</sup> Xiangwei Yin,<sup>4,5,§</sup> and Cong Zhang<sup>1,¶</sup>

<sup>1</sup>*College of Physics, Sichuan University, Chengdu 610065, China*

<sup>2</sup>*Institute of High Energy Physics, Chinese Academy of Sciences, Beijing 100049, China*

<sup>3</sup>*Spallation Neutron Source Science Center, Dongguan 523803, China*

<sup>4</sup>*CAS Key Laboratory of Theoretical Physics, Institute of Theoretical Physics,  
Chinese Academy of Sciences, Beijing 100190, China*

<sup>5</sup>*School of Physical Sciences, University of Chinese Academy of Sciences, No. 19A Yuquan Road, Beijing 100049, China*

Dark Matter (DM) residing in a secluded sector with suppressed portal interaction could evade direct detections and collider searches. The indirect detections provide the most robust probe to this scenario. Depending on the structure of the dark sector, novel DM annihilation spectra are possible. The dark shower is a common phenomenon for particles in the dark sector, which take part in strong interactions and are boosted. In terms of simplified two-component DM models with vector portal interaction and pseudoscalar portal interaction, we study the dark showering effects for DM indirect detection. In those models, the heavier DM component which dominates the relic density annihilates into boosted lighter species. Together with the large coupling through which the lighter DM annihilates away in the early universe, the showered spectra provide as the smoking gun for the DM existence. Considering bounds obtained by the AMS-02 positron data and Fermi-LAT measurement of gamma-ray from the dwarf galaxies, we find the dark shower could open a new region of sensitivity that can not be probed before.

*Introduction* Although the dark matter (DM) existence is confirmed by many astrophysical observations, the signs of DM direct detections and collider searches remain null, thus putting very stringent constraints on the coupling between the DM and standard model (SM) particles. Meanwhile, the Weakly-Interacting-Massive-Particle (WIMP) miracle for DM relic abundance can be also realized with DM evolving in a thermal bath of dark sector particles which have order one couplings and weak scale masses. The hidden sector interacts with the SM through suppressed portal interactions, evading the DM direct detection and collider searches. Such a scenario is dubbed secluded DM model [1]. The existence of the hidden dark sector is well motivated by the fact that the DM is more abundant than particles from SM which has complex particle spectra and gauge structure, as well as theoretical perspectives such as string theory [2, 3], Hidden Valley (HV) models [4, 5], Dark QCD [6] and so on [7–9]. Generally, two or more particles in the dark sector could contribute to the measured DM density [10–14].

Due to the large coupling required by the thermal relic density, the DMs around the centers of galaxies can annihilate into dark sector particles efficiently. The signature of this annihilation process provides the most robust probe to the secluded DM sector, although its manifestation is highly dependent on the model setup. In the simplest case, the DMs annihilate directly into the mediators which are interacting feebly with SM particles [15]. Then the mediators can decay into SM particles, which induces stable photons, electrons/positrons, protons/antiprotons being detected in DM indirect detection experiments. In a non-trivial dark sector, the relic DMs may annihilate to other lighter dark states, with subsequent cascade decay [16, 17]. A large number of mediator particles can be

produced during the full evolution. Each additional dark sector particle in the cascade will increase the final state multiplicity, decrease the final state energy and broaden the final state spectra.

In this paper, we consider another novel indirect detection signal for the secluded DM model in the case of heavy relic DM annihilating into boosted stable dark species with much smaller masses. If the light species couple to mediators with relatively large coupling [18] and the mediator is much lighter than the relic DM, the hierarchy between the energy and mass of the light species will induce copious radiations of the mediator after the annihilation. The phenomenon is known as dark shower [19–22]. The boostness of light species opens up a new window to produce many kinds of light degrees of freedom in the dark sector. Probing the multiplicities and spectra of the radiated mediator can also help to reveal the inner structure of the dark sector. At the LHC, studies have shown that the dark jet from dark showering could be discriminated from QCD jet according to its substructures, such as semi-visible jet [23], emerging jet [24], and jet mass [25]. The dark showers have also been studied in the context of indirect detection, for explaining the galactic center excess [26–28]. However, those studies assume the dark shower evolution to be QCD-like, *i.e.* under unbroken  $SU(N)$  gauge symmetry, where the mass effects in the splitting function are not fully taken into account. In particular, the radiation of the longitudinal component of the gauge boson is not considered. There is a number of works that study the mass effects in the dark matter shower in a simplified dark  $U(1)$  model framework with  $Z'$  mediator [29–31] and in the supersymmetric framework with scalar mediator [32].

This work will illustrate the DM indirect detection signal induced by the dark shower in the frameworks of

two-component DM models with either vector or pseudoscalar mediator. There is a mass hierarchy between two DM particles and the heavier one contributes most of the DM relic [33]. The dark shower is simulated by the Monte-Carlo method where the mass (symmetry breaking) effects are fully taken into account in the shower evolution. Assuming the vector and pseudoscalar mediators to be dominantly decaying into electron-positron pair and photon-pair respectively, we survey the constraints from Fermi-LAT observations of dwarf spheroidal galaxies [34] and AMS02 measurement of positron flux [35, 36].

*Secluded dark matter models and their simplified scenarios* As candidates of multi-DM models, we consider a dark/hidden sector that has dark/hidden local or global symmetry and some SM singlet fields which are charged under a dark/hidden symmetry. Depending on the interactions between the hidden sector and the SM particles, typical scenarios of hidden sector models include the vector portal [37], the (pseudo)-scalar portal [38–40], and the neutrino portal [41–44]. In this study, we focus on our attention on the first two of these possibilities.

As simple UV complete models, we consider two models where one model provides vector portal while the other one induces pseudo-scalar portal interactions.

(i) *Vector portal model*: In this case we introduce a hidden local  $U(1)_H$  symmetry and SM singlet field contents

$$\text{Dirac fermions: } \chi (Q_\chi), \psi(Q_\psi), \quad \text{Scalar: } \varphi(2), \quad (1)$$

where the values inside brackets indicate  $U(1)_H$  charges of the fields. The hidden gauge symmetry is assumed to be spontaneously broken by the vacuum expectation value (VEV) of  $\varphi$ , denoted by  $v_\varphi$ , and we have massive  $Z'$  boson whose mass is  $m_{Z'} = 2g_H v_\varphi$ . In this study we omit to analyze scalar potential just requiring mixing between new scalar and the SM Higgs is small so that we can evade constraints from Higgs physics. The relevant Lagrangian for the Dirac fermions is

$$\bar{\chi}(i\not{D} - m_\chi)\chi + \bar{\psi}(i\not{D} - m_\psi)\psi, \quad (2)$$

where  $D_\mu\chi(\psi) = (\partial_\mu + iQ_{\chi(\psi)}g_H Z'_\mu)\chi(\psi)$  is the covariant derivative with  $g_H$  being gauge coupling of  $U(1)_H$ . In the following analysis, we parametrize gauge coupling with charge as  $g_{Z'\chi\chi(Z'\psi\psi)} \equiv Q_{\chi(\psi)}g_H$ . Here we require conditions  $|Q_\chi| \neq |Q_\psi|$ ,  $|2Q_\chi| \neq 2$ ,  $|2Q_\psi| \neq 2$  and  $|Q_\chi \pm Q_\psi| \neq 2$  so that we only have vector portal interaction, and  $\chi$  and  $\psi$  do not mix. Then we have remnant discrete symmetry  $Z_2^\chi \times Z_2^\psi$  where  $\chi$  and  $\psi$  are odd under each  $Z_2$ . Thus  $\chi$  and  $\psi$  are both stable. Note also that we assume  $Z'$  can decay into SM particles via small kinetic mixing effect inducing dark photon interactions.

(ii) *Pseudo-scalar portal model*: In this case we introduce a hidden global  $U(1)'_H \times Z_2^A \times Z_2^B$  symmetry where  $U(1)'_H$

is softly broken, and field contents are

$$\begin{aligned} \text{Fermions : } & \chi_L(0, +, -), \chi_R(Q, +, -), \\ & \psi_L(0, -, +), \psi_R(Q, -, +), \\ \text{Scalar : } & \varphi'(-Q, +, +), \end{aligned} \quad (3)$$

where values inside brackets indicate charges under  $(U(1)'_H, Z_2^A, Z_2^B)$ . Fermions  $\chi$  and  $\psi$  can have Dirac masses  $m_{\chi, \psi}$  since  $U(1)'_H$  is assumed to be softly broken, and they are both stable due to  $Z_2^A \times Z_2^B$  symmetry. We assume  $\varphi'$  develops a VEV. Then  $\varphi'$  induces pseudo-Goldstone boson associated with spontaneous breaking of  $U(1)'_H$  that has light mass  $m_A$  due to soft  $U(1)'_H$  breaking. We thus have pseudo-scalar portal interactions

$$\begin{aligned} \mathcal{L} \supset & y_\chi \bar{\chi}_L \chi_R \varphi' + y_\psi \bar{\psi}_L \psi_R \varphi' + h.c. \\ & \supset iA(y_{\chi\chi} \bar{\chi} \gamma_5 \chi + y_{A\psi\psi} \bar{\psi} \gamma_5 \psi), \end{aligned} \quad (4)$$

where  $\varphi' = (\phi + iA)/\sqrt{2}$  and  $y_{A\chi\chi(A\psi\psi)} \equiv y_{\chi(\psi)}/\sqrt{2}$ . We assume  $\phi$  is much heavier than  $A$  and pseudo-scalar portal interactions are dominant in DM annihilation processes. We assume  $A$  decays into two photons via effective interaction of  $AF_{\mu\nu}\tilde{F}^{\mu\nu}$  with  $\tilde{F}^{\mu\nu} = \epsilon^{\mu\nu\alpha\beta}F_{\alpha\beta}$  that can be induced if there is a dark sector field interacting with both  $A$  and photon.

In the above models DM is made of two WIMPs, and the interactions between the two DM species - so-called DM conversion [35, 36], modify the Boltzmann equation and impact the computation of the relic density. In the parameter region of interest, coupling constants are assumed to satisfy the relation  $g_{Z'\psi\psi} > g_{Z'\chi\chi}$  ( $y_{A\psi\psi} > y_{A\chi\chi}$ ) so that  $\psi$  couples to  $Z'(A)$  stronger than  $\chi$ . In addition we assume  $m_\chi > m_\psi$ . Then relic density of  $\chi$  is dominantly determined by annihilation cross section of  $\bar{\chi}\chi \rightarrow Z'(A) \rightarrow \bar{\psi}\psi$  process since that of  $\bar{\chi}\chi \rightarrow Z'Z'(AA)$  process is more suppressed by smaller coupling  $g_\chi(y_\chi)$ . The relic density in vector/pseudo-scalar model is thus roughly given by  $(\Omega h^2)_{V(A)} \sim (0.1\text{pb})/\langle\sigma v\rangle_{\bar{\chi}\chi \rightarrow Z'(A) \rightarrow \bar{\psi}\psi}$ . Therefore relic densities can be estimated by model parameters such that

$$\Omega h_V^2 \sim (0.05) \left( \frac{1.0}{g_{Z'\psi\psi}} \right)^2 \left( \frac{0.01}{g_{Z'\chi\chi}} \right)^2 \left( \frac{m_\chi}{20 \text{ GeV}} \right)^2, \quad (5)$$

$$\Omega h_A^2 \sim (0.1) \left( \frac{1.0}{y_{A\psi\psi}} \right)^2 \left( \frac{0.01}{y_{A\chi\chi}} \right)^2 \left( \frac{m_\chi}{20 \text{ GeV}} \right)^2, \quad (6)$$

where we assumed  $m_{\psi, A/Z'}^2 \ll m_\chi^2$  and ignored  $\psi$  and  $Z'/A$  masses for simplicity. When we set  $m_{Z'/A} < m_\psi$  the relic density of  $\psi$  will be much smaller than that of  $\chi$  since  $\psi$  couples to  $Z'/A$  stronger than  $\chi$  and  $\psi$  annihilates into  $Z'Z'(AA)$  efficiently. For a more accurate estimation of relic density, we apply two-component **micrOmegas** [45] implementing relevant interactions associated with DM candidates.

*Showering of boosted dark matter* From the annihilation of heavy relic DM  $\chi$ , boosted stable dark species including Dirac fermion  $\psi$  and mediator (vector  $Z'$  or pseudoscalar  $A$ ) are produced along with dark shower processes.

For a collinear time-like branching process  $a \rightarrow b + c$ , where the off-shell particle  $a$  is in the final state of a preceding hard process, we parameterize the four-momentum of these particles by

$$P_a^\mu = (P, 0, 0, P - \frac{k_\perp^2 + \bar{z}m_b^2 + zm_c^2}{2z\bar{z}P}), \quad (7)$$

$$P_b^\mu = (zP, k_\perp, 0, zP - \frac{k_\perp^2 + m_b^2}{2zP}), \quad (8)$$

$$P_c^\mu = (\bar{z}P, -k_\perp, 0, \bar{z}P - \frac{k_\perp^2 + m_c^2}{2\bar{z}P}), \quad (9)$$

where  $\bar{z} = 1 - z$ ,  $z$  ranges in  $(0, 1)$ , and  $P^2 \gg k_\perp^2, m_i^2$  ( $i = a, b, c$ ). When ignoring terms proportional to  $\frac{k_\perp^2 \text{ or } m_i^2}{P^2}$  ( $i = a, b, c$ ),  $b$  and  $c$  are on-shell, but  $a$  is off-shell with virtuality  $Q$  satisfying

$$Q^2 = \frac{k_\perp^2 + \bar{z}m_b^2 + zm_c^2}{z\bar{z}}. \quad (10)$$

The differential cross section of the hard process followed by the branching of  $a \rightarrow b + c$  can be expressed as

$$d\sigma_{X,bc} \simeq d\sigma_{X,a} \times d\mathcal{P}_{a \rightarrow b+c}, \quad (11)$$

where  $X$  stands for other particles in the final state of the hard process besides  $a$ . And  $d\mathcal{P}_{a \rightarrow b+c}$  is the differential splitting function for the  $a \rightarrow b + c$  branching, which can be expressed as

$$\frac{d\mathcal{P}_{a \rightarrow b+c}}{dz d \ln Q^2} \approx \frac{1}{N} \frac{1}{16\pi^2} \frac{Q^2}{(Q^2 - m_a^2)^2} |M_{\text{split}}|^2, \quad (12)$$

where  $N = 2$  if  $b$  and  $c$  are identical particles otherwise  $N = 1$ . And  $|M_{\text{split}}|^2$  is the matrix-element square of the  $a \rightarrow b + c$  branching process by considering the amputated  $a \rightarrow b + c$  Feynman diagram with on-shell particle polarizations.

With two different types of mediators (vector boson  $Z'$  and pseudoscalar  $A$ ), the  $|M_{\text{split}}|^2$  of branchings from  $\psi$  and mediator is listed in Tab. I and II, respectively. We have to emphasize that the  $|M_{\text{split}}|^2$  in these tables have been averaged (summed) over polarizations of the corresponding initial (final) particles within the requirement of fermion helicity relation given in the second column. And according to the Ref. [46], we have eliminated terms proportional to  $(Q^2 - m_a^2)$  in  $M_{\text{split}}$  of processes involving the longitudinal mode of  $Z'$ .

Considering all the possible branching of  $a$ , the famous Sudakov form factor

$$\Delta_a(Q_{\text{max}}; Q_{\text{min}}) = \exp \left[ - \sum_{bc} \int_{\ln Q_{\text{min}}^2}^{\ln Q_{\text{max}}^2} d \ln Q^2 \int_{z_{\text{min}}(Q)}^{z_{\text{max}}(Q)} dz \frac{d\mathcal{P}_{a \rightarrow b+c}(z, Q)}{dz d \ln Q^2} \right], \quad (13)$$

Process	$\lambda_a(\lambda_b), \lambda_c$	$ M_{\text{split}} ^2$
$Z'_T \rightarrow \psi + \bar{\psi}$	$\lambda_b = \lambda_c$	$2g_{Z'\psi\psi}^2 \frac{m_\psi^2}{z(1-z)}$
$Z'_T \rightarrow \psi + \bar{\psi}$	$\lambda_b = -\lambda_c$	$2g_{Z'\psi\psi}^2 (z^2 + (1-z)^2) (Q^2 - \frac{m_\psi^2}{z(1-z)})$
$Z'_L \rightarrow \psi + \bar{\psi}$	$\lambda_b = \lambda_c$	0
$Z'_L \rightarrow \psi + \bar{\psi}$	$\lambda_b = -\lambda_c$	$8g_{Z'\psi\psi}^2 m_{Z'}^2 z(1-z)$
$\psi/\bar{\psi} \rightarrow Z'_T + \psi/\bar{\psi}$	$\lambda_a = \lambda_c$	$2g_{Z'\psi\psi}^2 \frac{(1+(1-z)^2)}{z} (Q^2 - \frac{m_{Z'}^2(1-z) + m_\psi^2 z}{z(1-z)})$
$\psi/\bar{\psi} \rightarrow Z'_T + \psi/\bar{\psi}$	$\lambda_a = -\lambda_c$	$2g_{Z'\psi\psi}^2 \frac{m_\psi^2 z^2}{1-z}$
$\psi/\bar{\psi} \rightarrow Z'_L + \psi/\bar{\psi}$	$\lambda_a = \lambda_c$	$4g_{Z'\psi\psi}^2 \frac{m_{Z'}^2(1-z)}{z^2}$
$\psi/\bar{\psi} \rightarrow Z'_L + \psi/\bar{\psi}$	$\lambda_a = -\lambda_c$	0

TABLE I. The  $|M_{\text{split}}|^2$  of branchings from  $\psi$  and mediator when the mediator is vector boson  $Z'$ .  $Z'_T$  and  $Z'_L$  are the transverse and longitudinal polarization modes of  $Z'$ , respectively. The fermion helicity is labelled by  $\lambda$ .

Process	$\lambda_a(\lambda_b), \lambda_c$	$ M_{\text{split}} ^2$
$A \rightarrow \psi + \bar{\psi}$	$\lambda_b = \lambda_c$	$2y_{A\psi\psi}^2 (Q^2 - \frac{m_\psi^2}{z(1-z)})$
$A \rightarrow \psi + \bar{\psi}$	$\lambda_b = -\lambda_c$	$2y_{A\psi\psi}^2 \frac{m_\psi^2}{z(1-z)}$
$\psi/\bar{\psi} \rightarrow A + \psi/\bar{\psi}$	$\lambda_a = \lambda_c$	$y_{A\psi\psi}^2 \frac{m_\psi^2 z^2}{1-z}$
$\psi/\bar{\psi} \rightarrow A + \psi/\bar{\psi}$	$\lambda_a = -\lambda_c$	$y_{A\psi\psi}^2 (Q^2 z - \frac{m_\psi^2 z + m_A^2(1-z)}{1-z})$

TABLE II. The  $|M_{\text{split}}|^2$  of branchings from  $\psi$  and mediator when the mediator is pseudoscalar  $A$ . The fermion helicity is labelled by  $\lambda$ .

gives  $a$ 's probability of evolving from  $Q_{\text{max}}$  to  $Q_{\text{min}}$  with no branching. The allowed  $z$  range at  $Q$  is given by [32]

$$z_{\text{min}}(Q) = \frac{1 - v_c}{1 + v_c/v_b}, \quad (14)$$

$$z_{\text{max}}(Q) = \frac{1 + v_c}{1 + v_c/v_b}, \quad (15)$$

with

$$v_b = \sqrt{1 - \left( \frac{2m_b Q}{Q^2 + m_b^2 - m_c^2} \right)^2}, \quad (16)$$

$$v_c = \sqrt{1 - \left( \frac{2m_c Q}{Q^2 + m_c^2 - m_b^2} \right)^2}. \quad (17)$$

A numerical Monte Carlo method with Markov chain based on the Sudakov factors of  $\psi$  and mediator ( $Z'$  or  $A$ ) is used to study the dark parton shower in this work. When evolving from a high virtuality scale  $Q_{\text{max}}$ , chosen to be the CM-frame energy of the hard annihilation process of  $\chi$ , down to a low scale  $Q_{\text{min}}$  with small  $Q$  steps, if the  $a \rightarrow b + c$  branching occurs at some  $Q$ , the evolution will be carried on with both the daughters  $b$  and  $c$ .

*Indirect detection signals* Considering the dark shower, the annihilation of relic DM ( $\chi$ ) for the vector portal model will induce multiple  $Z'$  emissions as illustrated in Fig. 1. Similarly, there will be multiple pseudoscalar signal for the pseudoscalar portal model, except that the  $\chi\chi \rightarrow AA$  annihilation is  $p$ -wave suppressed.

The dwarf spheroidal satellite galaxies (dSphs) of the Milky Way contain a substantial DM component[47, 48] and are expected to produce some of the brightest signals

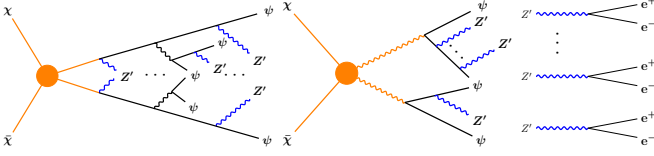


FIG. 1. Indirect detection signature for  $\chi\chi$  annihilation in the vector portal model.

of DM annihilation, thus they can be used to set stringent limits on the pseudoscalar portal DM model. We use the publicly released bin-by-bin likelihoods of each dwarf in Ref. [49]. Treating the energy bins as independent, the multiplication of likelihoods of all of the bins gives the likelihood for a given dwarf  $i$ ,  $\mathcal{L}_i(\Phi_\gamma|\mathcal{D}_i)$ , in which  $\Phi_\gamma$  is the gamma-ray flux of the DM model and  $\mathcal{D}_i$  is the data. Finally, the full likelihood is obtained by multiplying the likelihood of the following 15 dwarfs: Bootes I, Canes Venatici II, Carina, Coma Berenices, Draco, Fornax, Hercules, Leo II, Leo IV, Sculptor, Segue 1, Sextans, Ursa Major II, Ursa Minor, and Willman 1.

Giving the energy spectra of gamma-rays per annihilation of heavier DM ( $\chi$ ) as discussed above, the differential flux of gamma-rays at the location of the earth is given by [50]

$$\frac{d\Phi_\gamma}{dE_\gamma} = \frac{1}{\eta} \frac{1}{4\pi} \frac{1}{m_\chi^2} J \sum_{f=\psi, A} \langle \sigma_A v \rangle_f \frac{dN_\gamma^f}{dE_\gamma}, \quad (18)$$

where  $\eta$  is 4 for Dirac DM and 2 for Majorana DM. The  $J$ -factor is the line-of-sight (l.o.s.) integral through the DM distribution integrated over a solid angle. We adopt the value of  $J$ -factors for the Milky Way dSphs in Ref. [49], which are calculated assuming an NFW density profile and integrated over a circular region with a solid angle of  $\Delta\Omega \sim 2.4 \times 10^{-4}$  sr. The  $dN_\gamma^f/dE_\gamma$  is the energy spectrum of gamma-rays per annihilation in the channel with final state  $f$ . The thermal averaged annihilation cross section  $\langle \sigma_A v \rangle_A$  (measured in  $\text{cm}^3 \text{s}^{-1}$ ) of the channel  $\chi\chi \rightarrow AA$  is  $p$ -wave suppressed, while the cross section for  $s$ -wave annihilation  $\chi\chi \rightarrow \psi\psi$  is given by

$$\langle \sigma_A v \rangle_\psi = y_{A\chi\chi}^2 y_{A\psi\psi}^2 \frac{m_\chi \sqrt{m_\chi^2 - m_\psi^2}}{2\pi(m_A^2 - 4m_\chi^2)^2}. \quad (19)$$

The AMS measurement of positron flux [51–53] could set stringent limits to the vector portal model. In contrast to the gamma-ray, positrons propagate through the galactic magnetic field are deflected by its irregularities, which need to be investigated numerically. Refs. [50, 54] provide essential propagation functions that encode all the intervening astrophysics. Thus, the differential flux at the location of the earth can be calculated by convoluting the spectra at production with the propagation

functions:

$$\begin{aligned} \frac{d\Phi_{e^+}}{dE_{e^+}}(E) &= \frac{v_{e^+}}{4\pi b(E, r_{\text{sun}})} \frac{1}{\eta} \left( \frac{\rho(r_{\text{sun}})}{m_\chi} \right)^2 \\ &\times \sum_{f=\psi, Z'} \langle \sigma v \rangle_f \int_E^{m_\chi} dE_s \frac{dN_{e^+}^f}{dE}(E_s) I(E, E_s, r_{\text{sun}}). \end{aligned} \quad (20)$$

The information on the galactic DM density profile and propagation of positrons is summarized in the halo function  $I(E, E_s, r_{\text{sun}})$ , where  $E_s$  is the energy at production and  $r_{\text{sun}}$  is the Earth distance to the galactic center. The energy loss coefficient function  $b(E, r_{\text{sun}})$  depicts the energy loss at the location of the earth due to several processes, such as synchrotron radiation and Inverse Compton scattering (ICS) on CMB photons and on infrared or optical galactic starlight. We adopt the MED model [55, 56] for the propagation parameters and MF1 [57] for the magnetic field configuration. Different choices of parameters can affect the flux up to one order of magnitude. Moreover,  $r_s = 24.42$  kpc and  $\rho_s = 0.184 \text{ GeV/cm}^3$  are adopted in the NFW density profile. The thermal averaged annihilation cross sections for the vector portal model are given by

$$\langle \sigma v \rangle_f = \begin{cases} g_{Z'\chi\chi}^4 \frac{(m_\chi^2 - m_{Z'}^2)^{3/2}}{4\pi m_\chi (m_{Z'}^2 - 2m_\chi^2)^2} & \chi\chi \rightarrow Z'Z' \\ g_{Z'\chi\chi}^2 g_{Z'\psi\psi}^2 \frac{\sqrt{m_\chi^2 - m_\psi^2} (2m_\chi^2 + m_\psi^2)}{2\pi m_\chi (m_{Z'}^2 - 4m_\chi^2)^2} & \chi\chi \rightarrow \psi\psi \end{cases}. \quad (21)$$

In order to derive the upper limits on the cross sections or couplings, we assume the positron flux from AMS-02 measurement arises solely from the astrophysical backgrounds and fit the  $\log(\Phi_{e^+})$  of background with degree 6 polynomial of  $\log E_{e^+}$ . Defining  $\chi^2 = \sum_i \frac{\Phi_i^{\text{model}}(\alpha) - \Phi_i^{\text{data}}}{\sigma_i^2}$ , where  $\Phi_i^{\text{model}}$ ,  $\Phi_i^{\text{data}}$  and  $\sigma_i$  represent the flux predicted by the polynomial function with parameters  $\{\alpha\}$ , the measured flux and the total uncertainties (systematic and statistical uncertainties added in quadrature) in the  $i$ -th energy bin respectively. And the best-fit values for the polynomial parameter and  $\chi^2$  are denoted by  $\{\alpha_{\text{bf}}\}$  and  $\chi_{\text{bf}}^2$ . Then we add the DM-induced flux in Eq. (20) to the background and fit the stacked flux allowing the parameters to float within 30% of  $\{\alpha_{\text{bf}}\}$ . The 95% C.L. limit can be obtained by  $\chi^2(\langle \sigma v \rangle_{95}) \equiv \chi_{\text{bf}}^2 + 2.71$ . This methodology has been widely used in literature [17, 58, 59].

*Constraints and discussion* The above methodology has been applied to the full parameter space of our models. The details for some benchmark points are provided in the supplemental material. In Fig. 2, we show the bounds from AMS-02 (shaded region) and Fermi-LAT observations of dwarf galaxies (solid line) in  $m_\psi$ - $g_\psi$  plane with various  $m_\chi$ s where  $g_\psi = g_{Z'\psi\psi}$  ( $y_{A\psi\psi}$ ) for vector (pseudoscalar) mediator scenario.

The Fermi-LAT bound and the upper exclusion region of AMS-02 are induced by the dark showers subsequent

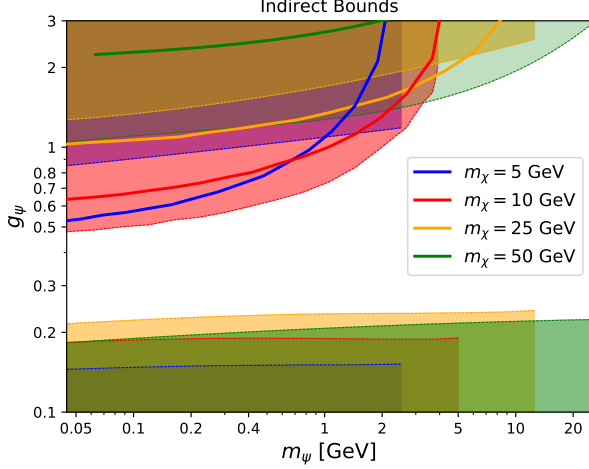


FIG. 2. Indirect detection bounds from Fermi-LAT for pseudoscalar portal model (solid line) and from AMS-02 for vector portal model (shaded region).

to the annihilation of  $\chi\chi \rightarrow \psi\psi$ . In the pseudoscalar portal model, giving the correct DM relic density (the parameter relation approximately satisfies Eq. (6)), the gamma-ray flux (in Eq. (18)) is proportional to  $g_\psi^2/m_\chi^2$  in the region  $m_{\psi,A} \ll m_\chi$ . As a result, the sensitivity of Fermi-LAT degrades with increasing  $m_\chi$  in the small  $m_\psi$  region. In the vector portal model, the positron flux from  $\chi\chi \rightarrow \psi\psi$  annihilation is proportional to  $g_\psi^2/m_\chi^2$  which is similar to the gamma-ray flux of the pseudoscalar model (more details are provided in supplementary). The bounds in the small  $m_\psi$  region fluctuate with increasing  $m_\chi$  mainly attributed to the features of the AMS-02 data and the  $\chi^2$  test method. In both cases, the larger mass splitting between the  $\chi$  and  $\psi$  can lead to stronger dark showering effects, *i.e.* higher particle multiplicity. Thus the sensitivities become stronger with decreasing  $m_\psi$  for a given  $m_\chi$ . The additional  $s$ -wave annihilation  $\chi\chi \rightarrow Z'Z'$  in the vector portal model induces the lower exclusion region of AMS-02, which is the only detectable region if dark showering effects are ignored. The flux of this channel is proportional to  $1/g_\psi^4$  in the region with  $m_{\psi,Z'} \ll m_\chi$  and  $g_{Z'\psi\psi} \lesssim \mathcal{O}(1)$  so that the bounds are relatively stable with respect to the variation of  $m_\chi$ .

This work was supported in part by the National Natural Science Foundation of China under grants No. 11905149 and No.12247119, by the Fundamental Research Funds for the Central Universities.

\* jmli@scu.edu.cn  
† nomura@scu.edu.cn  
‡ peijunle@ihep.ac.cn  
§ yinxiangwei@itp.ac.cn  
¶ zhangcong.phy@gmail.com

- [1] Maxim Pospelov, Adam Ritz, and Mikhail B. Voloshin, “Secluded WIMP Dark Matter,” *Phys. Lett. B* **662**, 53–61 (2008), arXiv:0711.4866 [hep-ph].
- [2] Luis E. Ibanez, Jihn E. Kim, Hans Peter Nilles, and F. Quevedo, “Orbifold Compactifications with Three Families of  $SU(3) \times SU(2) \times U(1)^{**n}$ ,” *Phys. Lett. B* **191**, 282–286 (1987).
- [3] Michael Blaszczyk, Stefan Groot Nibbelink, Orestis Loukas, and Saul Ramos-Sanchez, “Non-supersymmetric heterotic model building,” *JHEP* **10**, 119 (2014), arXiv:1407.6362 [hep-th].
- [4] Matthew J. Strassler and Kathryn M. Zurek, “Echoes of a hidden valley at hadron colliders,” *Phys. Lett. B* **651**, 374–379 (2007), arXiv:hep-ph/0604261.
- [5] Tao Han, Zongguo Si, Kathryn M. Zurek, and Matthew J. Strassler, “Phenomenology of hidden valleys at hadron colliders,” *JHEP* **07**, 008 (2008), arXiv:0712.2041 [hep-ph].
- [6] Yang Bai and Pedro Schwaller, “Scale of dark QCD,” *Phys. Rev. D* **89**, 063522 (2014), arXiv:1306.4676 [hep-ph].
- [7] Miguel Escudero, Samuel J. Witte, and Dan Hooper, “Hidden Sector Dark Matter and the Galactic Center Gamma-Ray Excess: A Closer Look,” *JCAP* **11**, 042 (2017), arXiv:1709.07002 [hep-ph].
- [8] Patrick Barnes, Zachary Johnson, Aaron Pierce, and Bibhushan Shakya, “Simple Hidden Sector Dark Matter,” *Phys. Rev. D* **102**, 075019 (2020), arXiv:2003.13744 [hep-ph].
- [9] Torsten Bringmann, Paul Frederik Depsta, Marco Hufnagel, and Kai Schmidt-Hoberg, “Precise dark matter relic abundance in decoupled sectors,” *Phys. Lett. B* **817**, 136341 (2021), arXiv:2007.03696 [hep-ph].
- [10] Kathryn M. Zurek, “Multi-Component Dark Matter,” *Phys. Rev. D* **79**, 115002 (2009), arXiv:0811.4429 [hep-ph].
- [11] Stefano Profumo, Kris Sigurdson, and Lorenzo Ubaldi, “Can we discover multi-component WIMP dark matter?” *JCAP* **12**, 016 (2009), arXiv:0907.4374 [hep-ph].
- [12] Daniel Feldman, Zuowei Liu, Pran Nath, and Gregory Peim, “Multicomponent Dark Matter in Supersymmetric Hidden Sector Extensions,” *Phys. Rev. D* **81**, 095017 (2010), arXiv:1004.0649 [hep-ph].
- [13] Mayumi Aoki, Michael Duerr, Jisuke Kubo, and Hiroshi Takano, “Multi-Component Dark Matter Systems and Their Observation Prospects,” *Phys. Rev. D* **86**, 076015 (2012), arXiv:1207.3318 [hep-ph].
- [14] Alexandre Poulin and Stephen Godfrey, “Multicomponent dark matter from a hidden gauged  $SU(3)$ ,” *Phys. Rev. D* **99**, 076008 (2019), arXiv:1808.04901 [hep-ph].
- [15] Patrick Barnes, Zachary Johnson, Aaron Pierce, and Bibhushan Shakya, “Indirect detection of secluded supersymmetric dark matter,” *Phys. Rev. D* **105**, 035005 (2022), arXiv:2106.09740 [hep-ph].
- [16] Gilly Elor, Nicholas L. Rodd, and Tracy R. Slatyer, “Multistep cascade annihilations of dark matter and the Galactic Center excess,” *Phys. Rev. D* **91**, 103531 (2015), arXiv:1503.01773 [hep-ph].
- [17] Gilly Elor, Nicholas L. Rodd, Tracy R. Slatyer, and Wei Xue, “Model-Independent Indirect Detection Constraints on Hidden Sector Dark Matter,” *JCAP* **06**, 024 (2016), arXiv:1511.08787 [hep-ph].
- [18] Yonit Hochberg, Eric Kuflik, Hitoshi Murayama, Tomer Volansky, and Jay G. Wacker, “Model for Thermal Relic

- Dark Matter of Strongly Interacting Massive Particles,” *Phys. Rev. Lett.* **115**, 021301 (2015), arXiv:1411.3727 [hep-ph].
- [19] Timothy Cohen, Mariangela Lisanti, Hou Keong Lou, and Siddharth Mishra-Sharma, “LHC Searches for Dark Sector Showers,” *JHEP* **11**, 196 (2017), arXiv:1707.05326 [hep-ph].
- [20] Timothy Cohen, Joel Doss, and Marat Freytsis, “Jet Substructure from Dark Sector Showers,” *JHEP* **09**, 118 (2020), arXiv:2004.00631 [hep-ph].
- [21] Simon Knapen, Jessie Shelton, and Dong Xu, “Perturbative benchmark models for a dark shower search program,” *Phys. Rev. D* **103**, 115013 (2021), arXiv:2103.01238 [hep-ph].
- [22] Guillaume Albouy et al., “Theory, phenomenology, and experimental avenues for dark showers: a Snowmass 2021 report,” (2022), arXiv:2203.09503 [hep-ph].
- [23] Timothy Cohen, Mariangela Lisanti, and Hou Keong Lou, “Semivisible Jets: Dark Matter Undercover at the LHC,” *Phys. Rev. Lett.* **115**, 171804 (2015), arXiv:1503.00009 [hep-ph].
- [24] Pedro Schwaller, Daniel Stolarski, and Andreas Weiler, “Emerging Jets,” *JHEP* **05**, 059 (2015), arXiv:1502.05409 [hep-ph].
- [25] Myeonghun Park and Mengchao Zhang, “Tagging a jet from a dark sector with Jet-substructures at colliders,” *Phys. Rev. D* **100**, 115009 (2019), arXiv:1712.09279 [hep-ph].
- [26] Marat Freytsis, Dean J. Robinson, and Yuhsin Tsai, “Galactic Center Gamma-Ray Excess through a Dark Shower,” *Phys. Rev. D* **91**, 035028 (2015), arXiv:1410.3818 [hep-ph].
- [27] Marat Freytsis, Simon Knapen, Dean J. Robinson, and Yuhsin Tsai, “Gamma-rays from Dark Showers with Twin Higgs Models,” *JHEP* **05**, 018 (2016), arXiv:1601.07556 [hep-ph].
- [28] David Curtin and Caleb Gemmell, “Indirect Detection of Dark Matter Annihilating into Dark Glueballs,” (2022), arXiv:2211.05794 [hep-ph].
- [29] Malte Buschmann, Joachim Kopp, Jia Liu, and Pedro A. N. Machado, “Lepton Jets from Radiating Dark Matter,” *JHEP* **07**, 045 (2015), arXiv:1505.07459 [hep-ph].
- [30] Minho Kim, Hye-Sung Lee, Myeonghun Park, and Mengchao Zhang, “Examining the origin of dark matter mass at colliders,” *Phys. Rev. D* **98**, 055027 (2018), arXiv:1612.02850 [hep-ph].
- [31] Junmou Chen, Pyungwon Ko, Hsiang-Nan Li, Jinmian Li, and Hiroshi Yokoya, “Light dark matter showering under broken dark  $U(1)$  — revisited,” *JHEP* **01**, 141 (2019), arXiv:1807.00530 [hep-ph].
- [32] Jinmian Li, Junle Pei, and Cong Zhang, “Multi-scalar signature of self-interacting dark matter in the NMSSM and beyond,” *JHEP* **09**, 151 (2021), arXiv:2104.10449 [hep-ph].
- [33] P. A. R. Ade et al. (Planck), “Planck 2015 results. XIII. Cosmological parameters,” *Astron. Astrophys.* **594**, A13 (2016), arXiv:1502.01589 [astro-ph.CO].
- [34] M. Ackermann et al. (Fermi-LAT), “Searching for Dark Matter Annihilation from Milky Way Dwarf Spheroidal Galaxies with Six Years of Fermi Large Area Telescope Data,” *Phys. Rev. Lett.* **115**, 231301 (2015), arXiv:1503.02641 [astro-ph.HE].
- [35] M. Aguilar et al. (AMS), “The Alpha Magnetic Spectrometer (AMS) on the international space station: Part II — Results from the first seven years,” *Phys. Rept.* **894**, 1–116 (2021).
- [36] M. Aguilar et al. (AMS), “Towards Understanding the Origin of Cosmic-Ray Positrons,” *Phys. Rev. Lett.* **122**, 041102 (2019).
- [37] Bob Holdom, “Two  $U(1)$ ’s and Epsilon Charge Shifts,” *Phys. Lett. B* **166**, 196–198 (1986).
- [38] Vanda Silveira and A. Zee, “SCALAR PHANTOMS,” *Phys. Lett. B* **161**, 136–140 (1985).
- [39] Brian Patt and Frank Wilczek, “Higgs-field portal into hidden sectors,” (2006), arXiv:hep-ph/0605188.
- [40] John McDonald, “Gauge singlet scalars as cold dark matter,” *Phys. Rev. D* **50**, 3637–3649 (1994), arXiv:hep-ph/0702143.
- [41] Peter Minkowski, “ $\mu \rightarrow e\gamma$  at a Rate of One Out of  $10^9$  Muon Decays?” *Phys. Lett. B* **67**, 421–428 (1977).
- [42] Murray Gell-Mann, Pierre Ramond, and Richard Slansky, “Complex Spinors and Unified Theories,” *Conf. Proc. C* **790927**, 315–321 (1979), arXiv:1306.4669 [hep-th].
- [43] Tsutomu Yanagida, “Horizontal gauge symmetry and masses of neutrinos,” *Conf. Proc. C* **7902131**, 95–99 (1979).
- [44] Rabindra N. Mohapatra and Goran Senjanovic, “Neutrino Mass and Spontaneous Parity Nonconservation,” *Phys. Rev. Lett.* **44**, 912 (1980).
- [45] G. Bélanger, F. Boudjema, A. Pukhov, and A. Semenov, “micrOMEGAs4.1: two dark matter candidates,” *Comput. Phys. Commun.* **192**, 322–329 (2015), arXiv:1407.6129 [hep-ph].
- [46] Junmou Chen, Tao Han, and Brock Tweedie, “Electroweak Splitting Functions and High Energy Showering,” *JHEP* **11**, 093 (2017), arXiv:1611.00788 [hep-ph].
- [47] Mario Mateo, “Dwarf galaxies of the Local Group,” *Ann. Rev. Astron. Astrophys.* **36**, 435–506 (1998), arXiv:astro-ph/9810070.
- [48] Alan W. McConnachie, “THE OBSERVED PROPERTIES OF DWARF GALAXIES IN AND AROUND THE LOCAL GROUP,” *The Astronomical Journal* **144**, 4 (2012).
- [49] M. Ackermann et al. (Fermi-LAT), “Searching for Dark Matter Annihilation from Milky Way Dwarf Spheroidal Galaxies with Six Years of Fermi Large Area Telescope Data,” *Phys. Rev. Lett.* **115**, 231301 (2015), arXiv:1503.02641 [astro-ph.HE].
- [50] Marco Cirelli, Gennaro Corcella, Andi Hektor, Gert Hutsi, Mario Kadastik, Paolo Panci, Martti Raidal, Filippo Sala, and Alessandro Strumia, “PPPC 4 DM ID: A Poor Particle Physicist Cookbook for Dark Matter Indirect Detection,” *JCAP* **03**, 051 (2011), [Erratum: *JCAP* **10**, E01 (2012)], arXiv:1012.4515 [hep-ph].
- [51] M. Aguilar et al. (AMS Collaboration), “Electron and positron fluxes in primary cosmic rays measured with the alpha magnetic spectrometer on the international space station,” *Phys. Rev. Lett.* **113**, 121102 (2014).
- [52] L. Accardo et al. (AMS Collaboration), “High statistics measurement of the positron fraction in primary cosmic rays of 0.5–500 GeV with the alpha magnetic spectrometer on the international space station,” *Phys. Rev. Lett.* **113**, 121101 (2014).
- [53] M. Aguilar et al., “The alpha magnetic spectrometer (ams) on the international space station: Part ii — results from the first seven years,” *Physics Reports* **894**, 1–116 (2021), the Alpha Magnetic Spectrometer (AMS)

on the International Space Station: Part II - Results from the First Seven Years.

- [54] <http://www.marcocirelli.net/PPPC4DMID.html>.
- [55] T. Delahaye, R. Lineros, F. Donato, N. Fornengo, and P. Salati, “Positrons from dark matter annihilation in the galactic halo: Theoretical uncertainties,” *Physical Review D* **77** (2008), 10.1103/physrevd.77.063527.
- [56] F. Donato, N. Fornengo, D. Maurin, P. Salati, and R. Taillet, “Antiprotons in cosmic rays from neutralino annihilation,” *Physical Review D* **69** (2004), 10.1103/physrevd.69.063501.
- [57] Jatan Buch, Marco Cirelli, Gaëlle Giesen, and Marco Taoso, “PPPC 4 DM secondary: A Poor Particle Physicist Cookbook for secondary radiation from Dark Matter,” *JCAP* **09**, 037 (2015), arXiv:1505.01049 [hep-ph].
- [58] Rebecca K. Leane, Tracy R. Slatyer, John F. Beacom, and Kenny C. Y. Ng, “GeV-scale thermal WIMPs: Not even slightly ruled out,” *Phys. Rev. D* **98**, 023016 (2018), arXiv:1805.10305 [hep-ph].
- [59] Koushik Dutta, Avirup Ghosh, Arpan Kar, and Biswarup Mukhopadhyaya, “A general study of decaying scalar dark matter: existing limits and projected radio signals at the SKA,” *JCAP* **09**, 005 (2022), arXiv:2204.06024 [hep-ph].



## SUPPLEMENTAL MATERIAL

### Benchmark points and dark shower spectra

To illustrate the dark showering effects for the DM annihilation in the pseudoscalar portal model and vector portal model, we select 5 benchmark points in each model and provide their details in Tab. III. The couplings  $g_{Z'\chi\chi}$  and  $y_{A\chi\chi}$  have been appropriately tuned to guarantee the relic density  $\Omega h_\chi^2 \sim 0.12$  and  $\Omega h_\psi^2 \ll \Omega h_\chi^2$ . Note that in calculating the bounds in Fig. 2, the couplings  $g_{Z'\chi\chi}$  and  $y_{A\chi\chi}$  are determined in more refined ways (logarithmically scanning the couplings  $g_{Z'\chi\chi}$  and  $y_{A\chi\chi}$  from  $10^{-3}$  with ratio  $10^{0.001}$  until the total density of  $\chi$  and  $\psi$  reaches 0.12). The  $\chi^2$  test value for each benchmark point of the vector portal model using the AMS-02 data, as well as the Fermi-LAT limit and the theoretical cross section for each benchmark point of the pseudoscalar portal model is provided.

	A	B	C	D	E
$m_\chi$ [GeV]	100	10	1000	10	1000
$m_\psi$ [GeV]	1	1	1	0.1	10
$g_{Z'\chi\chi}$	0.029	0.003	0.3	0.003	0.3
$y_{A\chi\chi}$	0.02	0.0022	0.22	0.0022	0.22
$\Omega_\chi$ [Vector]	0.111	0.115	0.101	0.115	0.101
$\Omega_\chi$ [Pseudoscalar]	0.128	0.118	0.108	0.117	0.108
$\Omega_\psi$ [Vector]	$2.03 \times 10^{-7}$	$2.17 \times 10^{-6}$	$2.24 \times 10^{-8}$	$2.17 \times 10^{-8}$	$1.93 \times 10^{-6}$
$\Omega_\psi$ [Pseudoscalar]	$1.54 \times 10^{-6}$	$2.74 \times 10^{-5}$	$3.07 \times 10^{-7}$	$1.21 \times 10^{-7}$	$1.39 \times 10^{-5}$
AMS-02 $\chi^2$	62.12	2001.9	50.0	2822.2	49.9
Fermi-LAT limit [cm <sup>2</sup> ]	$9.07533 \times 10^{-26}$	$5.28983 \times 10^{-27}$	$2.47742 \times 10^{-24}$	$2.50722 \times 10^{-27}$	$3.38713 \times 10^{-24}$
Model cross section [cm <sup>2</sup> ]	$4.18391 \times 10^{-26}$	$5.04364 \times 10^{-26}$	$5.06272 \times 10^{-26}$	$5.06253 \times 10^{-26}$	$5.06253 \times 10^{-26}$

TABLE III. Benchmark points for vector portal DM model and pseudoscalar DM model. In vector portal case, the coupling of  $\psi$  is chosen as  $\alpha_D \equiv g_{Z'\psi\psi}^2/4\pi = 0.2$  and the  $\chi_{\text{bf}}^2=49.8$ . In the pseudoscalar case, the coupling of  $\psi$  is  $y_{A\psi\psi} = 3$ . Varying the masses of mediators ( $Z'$  and  $A$ ) in the range  $\mathcal{O}(0.1)m_\psi$  gives similar results. In the last and second to the last row, the theoretical value and the Fermi-LAT bound of the  $\chi\chi \rightarrow \psi\psi$  annihilation cross section in the pseudoscalar portal model are presented.

In Fig. 3, we plot the spectra of positron and gamma-ray after the dark shower and mediator decay for the annihilation channels  $\chi\chi \rightarrow \psi\psi$  and  $\chi\chi \rightarrow Z'Z'$  in the vector portal model,  $\chi\chi \rightarrow \psi\psi$  in the pseudoscalar portal model. In the decay of the  $Z'$ , the polarization information has been taken into account. Comparing the left and right panels of the figure, we can find that the dark shower is copious for  $\psi$ , and it produces a harder spectrum in the pseudoscalar model than in the vector model. However, the shower of the boosted  $Z'$  in the  $\chi\chi \rightarrow Z'Z'$  channel is rare, giving the peak of  $E_{Z'}$  distribution at around  $m_\chi$ . The heights of the peaks are close to 2 because there are two  $Z'$  produced in each annihilation.

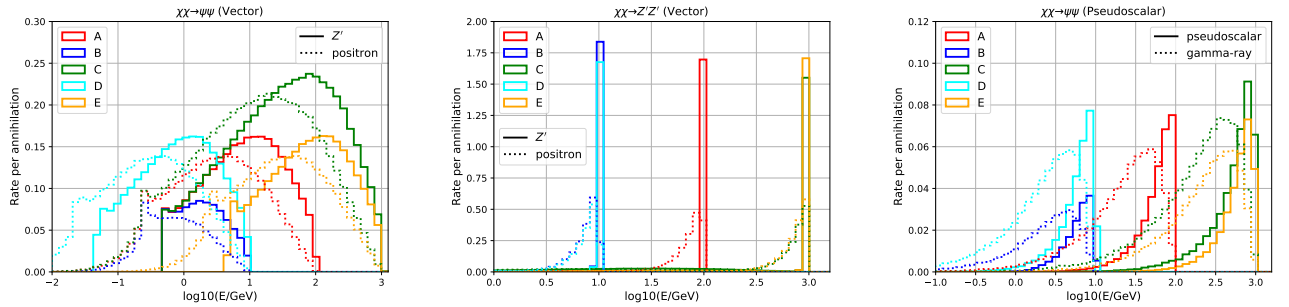


FIG. 3. Shower spectra for benchmark points. The mediator ( $Z'$  and pseudoscalar) masses are chosen to be half of the light DM  $\psi$  mass.

### Features of the positron flux

We discuss the features of the positron flux for the vector portal model in this section. The corresponding results for the gamma-ray flux in the pseudoscalar portal model are similar to those of the  $\chi\chi \rightarrow \psi\psi$  channel in the vector portal model.



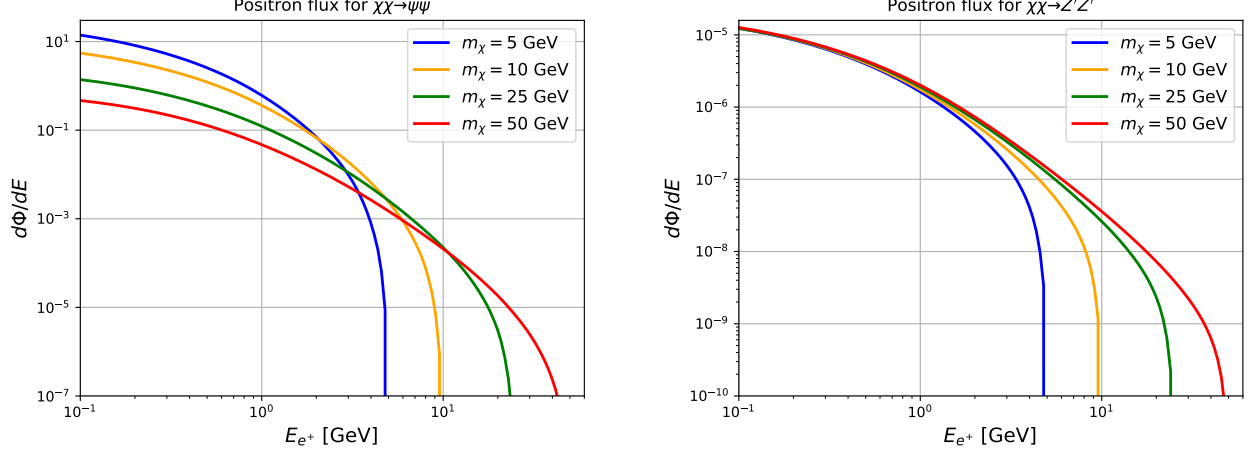


FIG. 4. Fluxes of positron near earth for the  $\chi\chi \rightarrow \psi\psi$  channel (left panel) and  $\chi\chi \rightarrow Z'Z'$  channel (right panel). The following parameters are chosen:  $m_\psi = 0.119$  GeV,  $m_{Z'} = 0.5m_\psi$ ,  $g_{Z'\psi\psi} = \sqrt{4\pi} \times 0.2$  and  $g_{Z'\chi\chi}$  is fixed by Eq. (5).

In the limit of  $m_\chi \gg m_{\psi,Z'}$  and assuming the correct relic density (with parameter relation satisfies Eq. (5)), the positron fluxes of  $\chi\chi \rightarrow \psi\psi$  channel ( $\frac{d\Phi}{dE}\big|_\psi$ ) and  $\chi\chi \rightarrow Z'Z'$  channel ( $\frac{d\Phi}{dE}\big|_{Z'}$ ) can be written as

$$\begin{aligned} \frac{d\Phi}{dE}\big|_\psi &= \frac{C_1(E)C_{2,Z'}}{m_\chi^2} \int_E^{m_\chi} dE_s \frac{dN_{e^+}^\psi}{dE}(E_s) I(E, E_s, r_{\text{sun}}) , \\ \frac{d\Phi}{dE}\big|_{Z'} &= \frac{C_1(E)C_{2,Z'}^2}{g_\psi^4} \int_E^{m_\chi} dE_s \frac{dN_{e^+}^{Z'}}{dE}(E_s) I(E, E_s, r_{\text{sun}}) , \end{aligned} \quad (22)$$

where  $dN_{e^+}^\psi/dE$  ( $\propto \alpha_D$ ) and  $dN_{e^+}^{Z'}/dE$  ( $\propto [1 + \frac{\alpha_D}{0.2}(N_D - 1)]$ ,  $N_D$  is the total number of simulated positrons for  $\alpha_D = 0.2$ ) are the spectra of the positron at the source for the  $\chi\chi \rightarrow \psi\psi$  channel and the  $\chi\chi \rightarrow Z'Z'$  channel respectively. For a given  $E$ , the halo function  $I(E, E_s, r_{\text{sun}})$  is relatively flat with respect to the energy at the source  $E_s$ . The factor  $C_{2,Z'}$  corresponds to the constant obtained with Eq. (5), i.e.  $C_{2,Z'} = g_{Z'\psi\psi}^2 g_{Z'\chi\chi}^2 / m_\chi^2$ . The factor  $C_1(E)$  collects the rest astrophysical parameters in Eq. (20).

Fig. 4 shows the positron fluxes around the earth for the  $\chi\chi \rightarrow \psi\psi$  channel and the  $\chi\chi \rightarrow Z'Z'$  channel with several given  $m_\chi$ . The flux for the  $\chi\chi \rightarrow \psi\psi$  channel is proportional to  $1/m_\chi^2$  thus is suppressed for heavier  $\chi$ . Although the dark shower becomes more copious for larger  $m_\chi$ , its effect is subdominant compared to that of the factor  $1/m_\chi^2$ . The difference in the positron flux of the  $\chi\chi \rightarrow Z'Z'$  channel for different  $\chi$  mass is attributed to the dark shower process. Heavier  $\chi$  will give rise to higher positron flux due to a longer evolution period. It should be noted that the relations in Eqs. (5) and (6) do not strictly hold according to our numerical calculation with `micrOmegas`. The  $g_\chi$  values could deviate from the ones that were used in Fig. 4. This will lead to overall rescalings by a factor of  $1 \pm \mathcal{O}(0.1)$  for those flux curves.